SPACE TELESCOPE SCIENCE INSTITUTE
Operated for NASA by AURA

WFC3 Instrument Science Report 2009-16

WFC3 SMOV Proposals 11419, 11426, 11431, and 11446: On-Orbit Darks

T. Borders, S. Baggett
November 16, 2009

ABSTRACT

This report summarizes the basic on-orbit characteristics of the SMOV UVIS dark frames. We investigate the dark current, the hot pixels, and describe the superdark. The average on-orbit dark current is measured to be 1.62e-/pix/hr with a standard deviation of 0.29 for chip#1 (amps A & B) and 1.70 e-/pix/hr with a standard deviation of 0.34 for chip#2 (amps C & D). Compared to ground tests, the dark current is $\sim$5x higher than expected yet well below the CEI spec of 20 e-/pix/hr. We discuss details of various checks to investigate possible causes for the higher rate. In addition to the overall increased dark rate we find a number of dark frames with extremely elevated dark current ($>$4 e-/pix/hr) for which we provide details of our investigation. We chose the hot pixel cutoff to be 20 e-/hr and measure a hot pixel rate of 530 hot pixels/day. We find that $>$70% of the hot pixels are fixed after an anneal.

Introduction

We report on the basic properties of the on-orbit darks, which, serve to monitor the on-orbit behavior of the dark current and the growth of hot pixels. Dark frames were obtained during SMOV (Servicing Mission Observatory Verification) after the Servicing Mission 4 in May 2009, from proposals 11419 (UVIS Detector Function Test/Gain), 11426 (UVIS Contamination Monitor), 11431 (UVIS Hot Pixel Anneal), and 11446 (UVIS Dark Rate, Noise, CTE). We analyzed the dark frames to monitor their dark current, hot pixels, and any anomalous features. Individual on-orbit dark frames as well as stacked superdark frames were compared to ground data to inspect for differences.

The Data

In Appendix A, Tables 7 - 8 list the dark files included in this study. These tables list for each observation: rootname, proposal id, date and time of observation, shutter blade used, filter, and the dark median (e-/pix/hr) for each chip. All images are full-frame, four-amp readout 1800 sec dark frames.

Analysis

Image Processing

All raw images were over-scan and bias corrected (DQICORR, BLEVCORR, and BIASCORR turned on) using *calwf3* version 27Apr2009. A Python script was used to automate the calibration with *calwf3* as reported in TIR 2008-01 (Martel et al. 2008a). The reference files used include t2c1553si_bpx.fits, t291659mi_ccd.fits, and q911321oi_osc.fits. Two on-orbit superbias frames were used for the bias calibrations depending on when the data were taken. For the darks taken before and after the first anneal on June 23rd, 2009 (MJD 55005.072917) the superbias b09061261_bia.fits, a combination of 61 frames, was used. Superbias b09061289_bia.fits, a combination of 89 frames, was used to calibrate the darks taken after the second anneal on July 20, 2009 (MJD 55032.399306).

We have tested various combinations of the cosmic ray (CR) rejection parameters in the CRREJTAB to determine an optimal set for stacking on-orbit darks. Two sets of CRREJTAB parameters summarized in Table 1 have been implemented for two different analysis procedures. One set is used to create a superdark from which to measure dark current and the other set of parameters is used for generating dark stacks for hot pixel analysis. While the parameters for the dark current are successful in flagging cosmic rays optimal for an analysis of the overall dark current they flag a large number of hot pixels providing an underestimate for the number of hot pixels. We tested the parameter space of the CRREJTAB in order to find a set of parameters to allow a more accurate determination of hot pixels. The biggest contributing factor was the sigmas used in the CRSIGMAS parameter used in cosmic ray rejection during each successive iteration. By increasing the CRSIGMAS, fewer hot pixels are flagged and the resulting stack provides a more accurate count of the hot pixels. We did not find the parameter SCALENSE to make any improvements to the masking: increasing SCALENSE merely increased the number of erroneous pixels flagged. We also decreased the CRRADIUS in order to decrease the number of hot pixels being flagged. One caveat to using the parameters for hot pixels analysis is that the outer perimeter of cosmic rays are not flagged properly. Using the IRAF routine CRGROW on the individual calibrated darks to grow the cosmic ray masks by 2 pixels thereby flags the perimeter of the cosmic rays being missed with the CCRREJTAB parameters.

Figure 1 shows a zoomed in region ($\sim$ 800 x 300 pixels) of image iaab01o7q

Table 1. *CRREJTAB parameters used for for dark current and hot pixel analysis*

	MEANEXP	SCALENSE	INGITGUES	SKYSUB	CRSIGMAS	CRRADIUS	CRTHRESH
		sec			none	pixels	
Dark Current Parameters	INDEF	3.0	minimum	none	6.5,5.5,4.5	2.1	0.5555
Hot Pixel Parameters	INDEF	3.0	minimum	none	40,39,38	0.5	0.5555

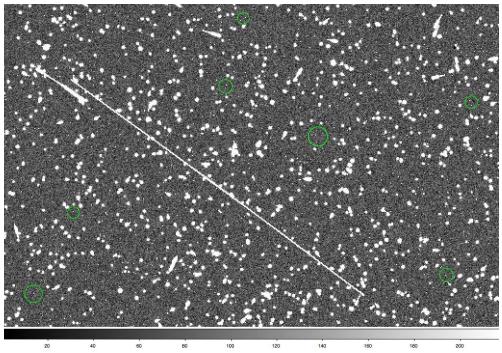

Figure 1. Zoomed in region ($\sim$ 800 x 300 pixels) of chip #2 of image iaab01o7q. Green circles highlight a few examples of hot pixels.

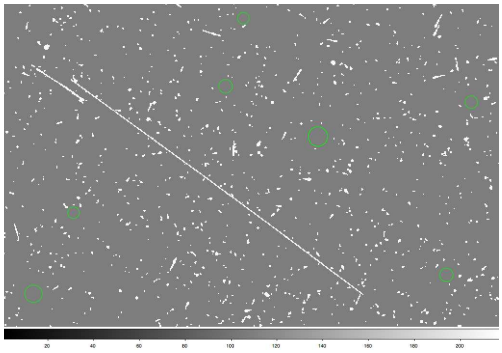

Figure 2. Mask of image iaab01o7q. Green circles highlight where hot pixels have been correctly ignored (unflagged).

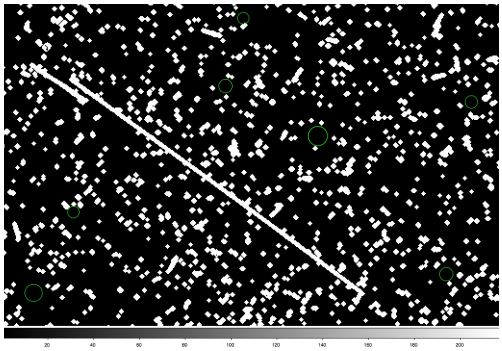

Figure 3. *Mask of image iaab01o7q after being processed by CRGROW.*

(chip #2) where a mix of cosmic rays and hot pixels can be seen as well as a long extended cosmic ray. The green circles highlight a few examples of hot pixels in this region. Figure 2 shows the mask of image iaab01o7q processed with the CRREJTAB parameters from Table 1 for hot pixel analysis. The same green circles from Figure 2 show that the hotpixels have been properly ignored (not flagged) in the mask. Notice that some of the larger cosmic rays in Figure 1 are not completely masked in Figure 2. Figure 3 shows the mask of image iaab01o7q that has been processed by CRGROW by growing the cosmic ray masks by 2 pixels, thus providing full masking of the entire

cosmic ray, including the wings.

Dark Current

For each dark frame, the dark current was computed from the good (unflagged) pixels for each chip and is shown in Tables 7 - 8 in Appendix A. We used a robust median, verified by fitting the distribution of dark values with a guassian. The average dark current for chip #1 is 1.62 e-/pix/hr with a standard deviation of 0.29 and for chip #2 the average dark current is 1.70 e-/pix/hr with a standard deviation of 0.34 excluding any darks whose current was 3σ above the mean. The dark current measured on the ground under thermal vacuum conditions was 0.3 e-/pix/hr. The on-orbit dark current is $\sim$1e-/pix/hr ($\sim$ 5x) higher than ground tests. The cause is not yet determined but a light leak around the shutter or radiation induced window glow are leading candidates.

Figure 4 shows a plot of time vs dark median (e-/pix/hr) for Chip #2 for each filter (data for Chip#1 is listed in Tables 7 - 8 in Appendix A). Anneals are represented by the dashed red vertical lines. From this figure there is no apparent trend for a filter dependent dark current, i.e one might expect higher levels in broader filters if there were a continual light leak.

There is a slight trend with time towards increasing dark current. A linear fit to the dark current is shown in Figure 4 with a fit of y=1.77E^{-4}x-8.06. According to this fit, the dark current is growing at a rate of less than 1 e-/pix/hr per year. This result is preliminary and more data are needed to continue this trending. We will continue to monitor the dark current during Cycle 17 where we will take 3x 900 sec darks daily.

Overall Elevated Darks

Throughout our analysis we performed a number of investigations in order to try and determine the cause of the overall higher dark rate (3-5x ground) as well as the extreme darks. Listed here are the results of those investigations with accompanying plots.

We investigated HST's orientation with respect to Earth as a function of dark current for any correlations. Figure 5 shows the median dark current (e-/pix/hr) as a function of V1 pointed at the bright Earth and Figure 6 shows the median dark current (e-/pix/hr) as a function of minutes that HST was above bright Earth. There does appear to be slight trend in Figure 5 of increasing dark current with increasing number of minutes VI is aimed at bright Earth implying that there may be a light leak, perhaps around the shutter. There does not, however, seem to be any strong correlation in Figure 6 with minutes HST is above bright Earth.

We checked for a correlation with dark current and hours since pinning exposure (see ISR 2009- Bowtie) shown in Figure 7 (i.e there has been a QE overshoot caused by the saturated flat) but we do not find any strong correlation.

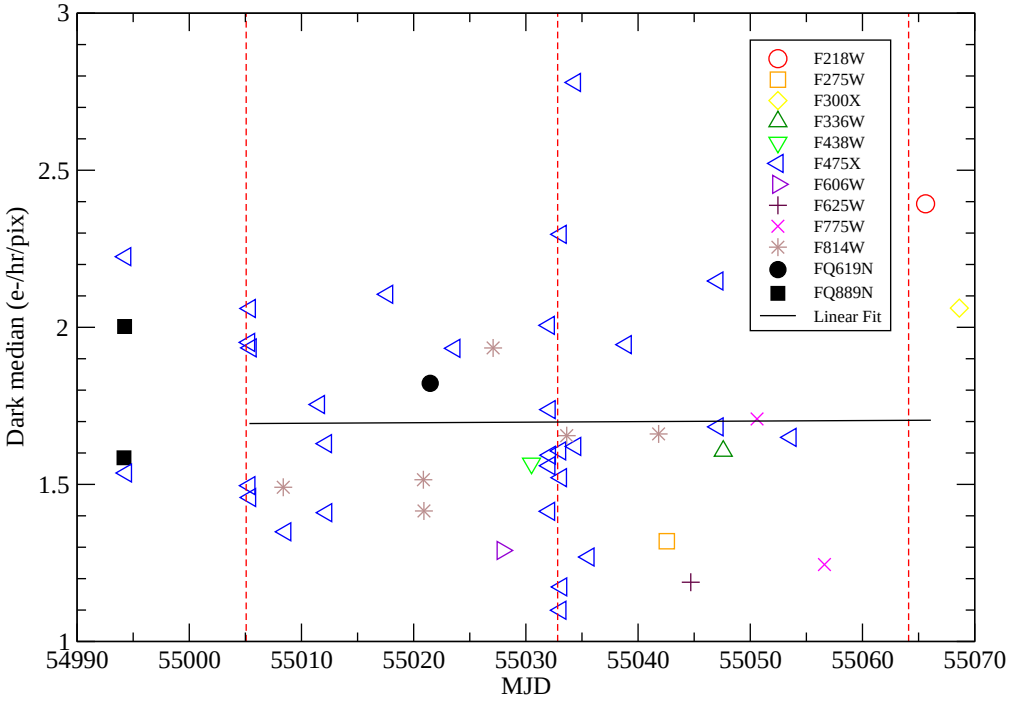

Figure 4. *Modified Julian Date vs dark median (e-/pix/hr) for Chip#2. Each filter is represented with a different symbol. Anneals are represented by the red vertical dashed lines. Linear fit of y=1.77E^{-4}x-8.06 is also shown.*

We investigated the bus voltage as a function of MJD, with dark overplotted as horizontal line two anomalously high darks shown in bottom row along with two normal darks at same phase with regard to bus voltage shown in Figure 8. The anomalous darks are not caused by voltage changes.

Shown in Figure 9 is the SAA dose and time since SAA, for various bins of dark median values. There is no trend of dark current with time since or dose during SAA.

Window temperature (data provided by Tom Wheeler) as a function of dark median (e-/pix/hr) is shown in Figure 10. There is no clear trend that the window temperature is a contributing factor to any increase in dark current.

Figure 11 plots the dark median for shutter A (green) vs shutter B (blue). The dark median does not appear to be shutter dependent if there is a light leak around the shutter, it's similar for both blades. The average mean value for shutter A is 1.67 (e-/pix/hr) with a standard deviation of 0.30 and the average mean for shutter B is 1.71

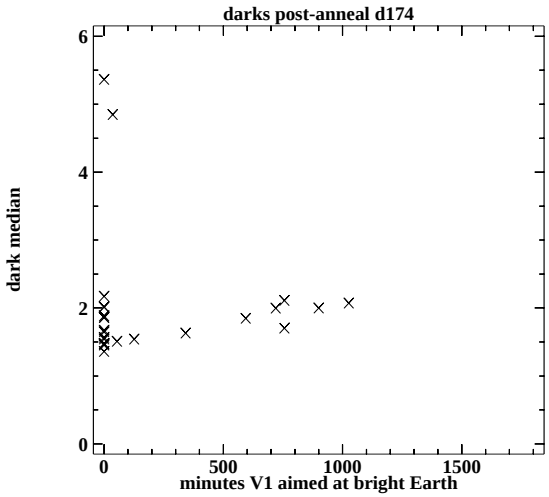

Figure 5. Median dark level (e-/pix/hr) vs minutes V1 was pointed at bright Earth

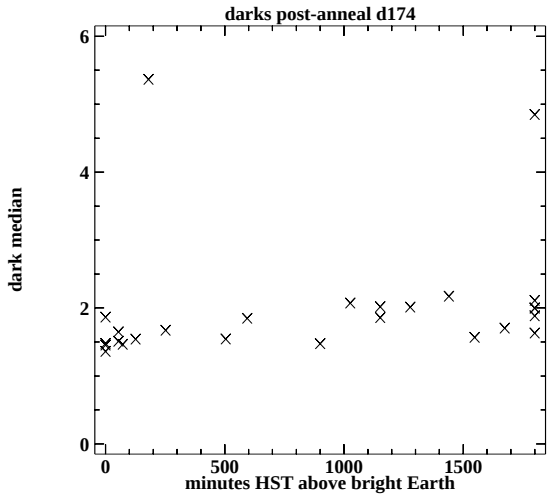

Figure 6. Median dark level (e-/pix/hr) vs minutes HST is above bright Earth

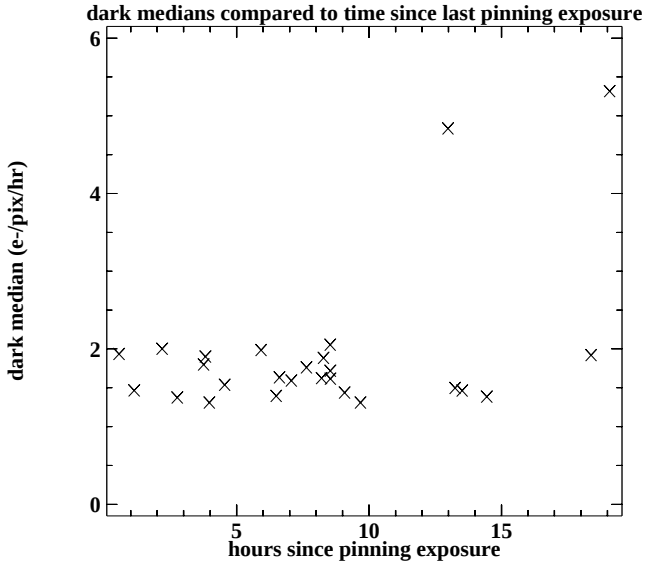

Figure 7. *Median dark current versus time since pinning exposure*

(e-/pix/hr) with a standard deviation of 0.41. The average value for both shutters is not statistically significant and thus there appears to be no dependance on shutter blade of a light leak around the shutter contributing to increased dark current.

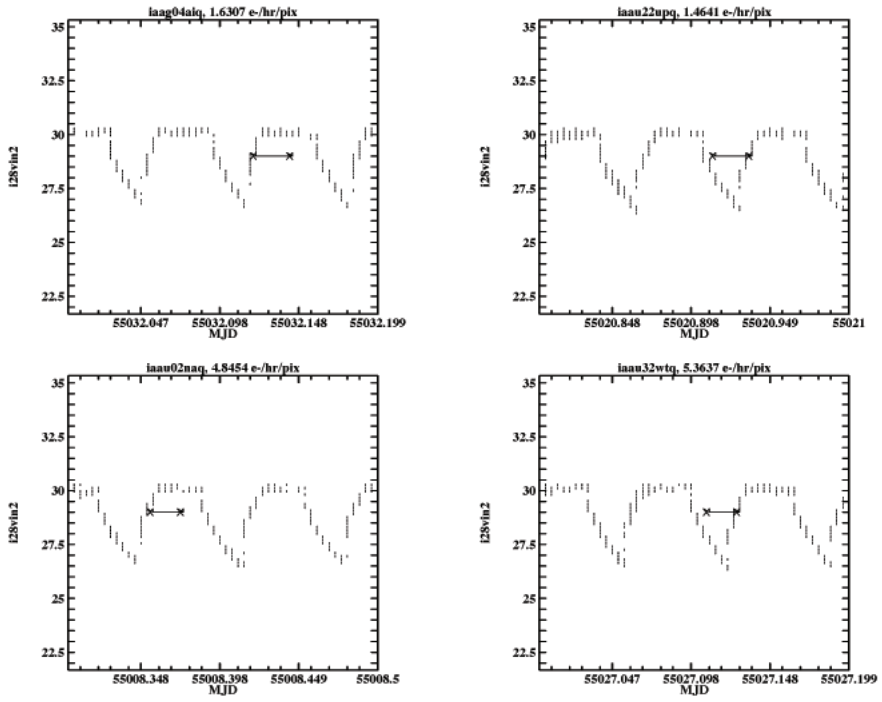

Figure 8. *MJD vs bus voltage, with dark overplotted as horizontal line. Two anomalously high darks are shown in bottom row along with two normal darks in top row, at the same phase with regard to bus voltage.*

Extreme Elevated Darks

There are a number of dark frames with extremely elevated dark current; these were excluded from the statistics for the average dark current. Table 4 lists the frames with elevated dark current along with proposal id, date and time of observation, shutter blade, filter, the dark median (e-/pix/hr) for each chip, and a comment about bright earth or dark earth occultation. Common to all of these exposures is a red filter in place and taken during bright earth occultation. Darks are taken with the UVIS shutter closed; in addition, whatever filter was used for the preceding exposure is left in place, as extra protection from any scattered light.

A binned 5x5 image is provided for each of the extremely elevated darks listed in Table 4 as well as a plot provided by Peter McCullough (private communication) which shows HST's orientation with respect to Earth. The green solid line represents the start of the observation and the red dashed lines for the end of the observation. The color of the squares is brown, purple, or yellow if HST is orbiting above the dark, twilight, or bright Earth The yellow filled circle inscribed within a squares represents the V1 axis

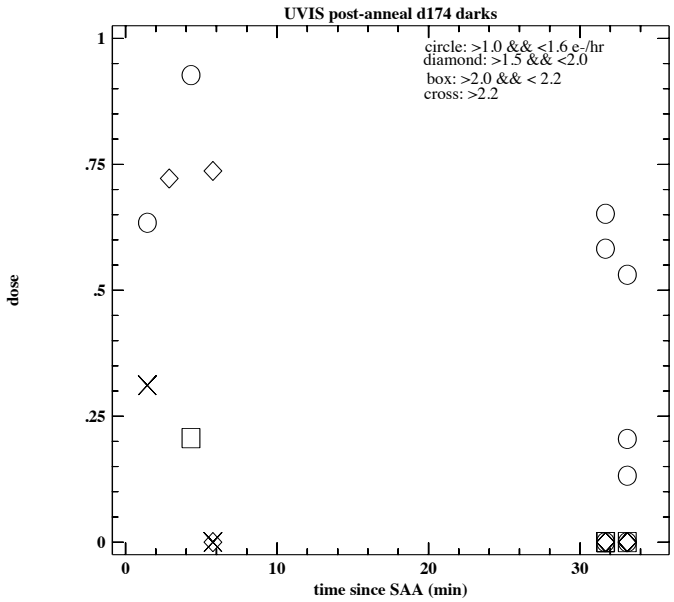

Figure 9. *SAA dose and time since SAA, for various bins of dark median values*

intersecting the Earth: i.e. HST is pointed directly at the bright Earth. More information on the generation and details of this plot can be found in ISR 2009 “Tools for predicting HST’s orientation with respect to Earth” by P. McCullough.

In Figure 12 a faint glow can be seen extending from the right hand side of the image iaau02naq in a vertical direction. Figure 13 shows that for image iaau02naq HST was pointed at bright earth for only a short period of time (7 min and 2 sec). Similarly in Figure 14 of image iaau32wtq a glow is extending from the right hand side of the image in a vertical direction and then extending across horizontally. Figure 15 shows that HST was pointed at bright earth for a short time (6 min and 7 sec). Image iaau52wxq has the highest dark current of 16.12 and 16.58 (e-/pix/hr) for chip#1 and chip#2. Figure 16 shows a binned 5x5 image of iaau52wxq where a glow extends from the right hand side of the image, indicating a possible light leak. As seen in Figure 17 this image has had its entire exposure occur during bright earth occultation. Figure 18 shows the binned 5x5 image of image iaab18ynq where there is a faint glow extending from the right hand side of the image. Figure19 shows that most of the exposure occurred during dark and bright earth occultation. Image iaab19zwq also has an especially extremely elevated dark current of 14.49 and 14.77(e-/pix/hr) for chip#1 and chip#2. Figure 20 shows the binned 5x5 image which shows a glow extending from the right hand side in a shape similar to iaau52wxq in Figure 16. Figure shows that like image iaau52wxq the entire exposure is in bright earth occulation.

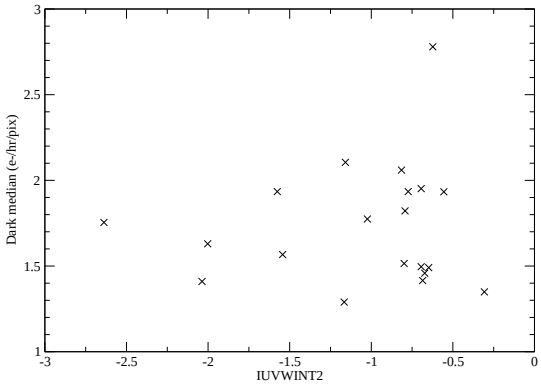

Figure 10. Window temperature vs dark median (e-/pix/hr). This plot covers period from June 23 - July 18, 2009.

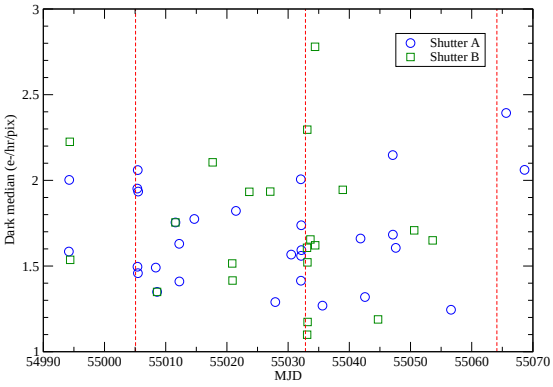

Figure 11. Modified Julian Date vs dark median (e-/pix/hr) where observations using shutter A are plotted in blue and shutter B in green.

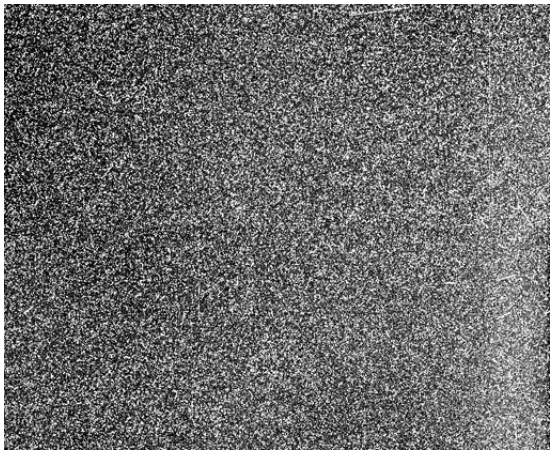

Figure 12. Binned 5x5 image of iaau02naq. A faint glow is extending from the right hand side indicating possible light leak.

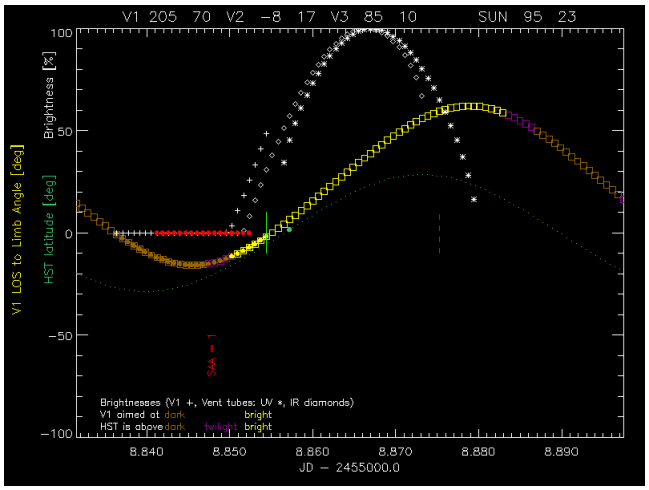

Figure 13. Plot showing HST's orientation with respect to Earth for image iaau02naq.

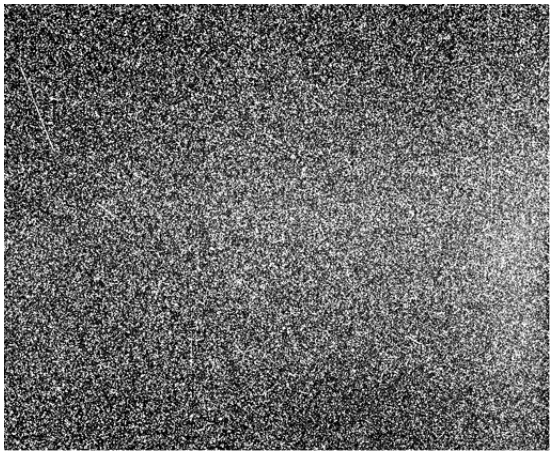

Figure 14. Binned 5x5 image of iaau32wtq. Glow extending from the right hand side indicates possible light leak.

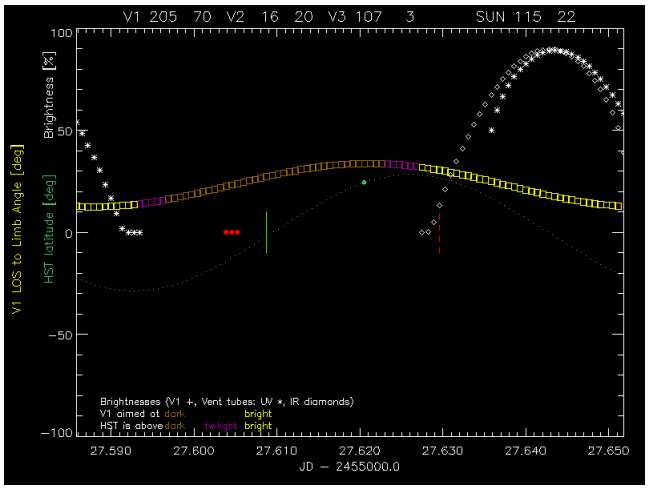

Figure 15. Plot showing HST's orientation with respect to Earth for image iaau32wtq.

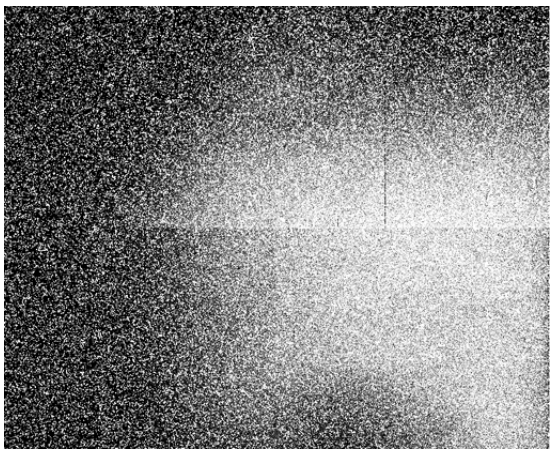

Figure 16. Binned 5x5 image of iaau52wxq. Glow extending from the right hand side indicates possible light leak.

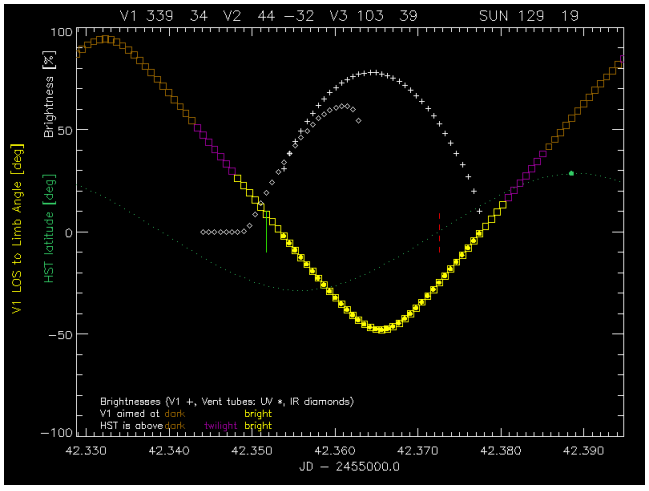

Figure 17. Plot showing HST's orientation with respect to Earth for image iaau52wxq.

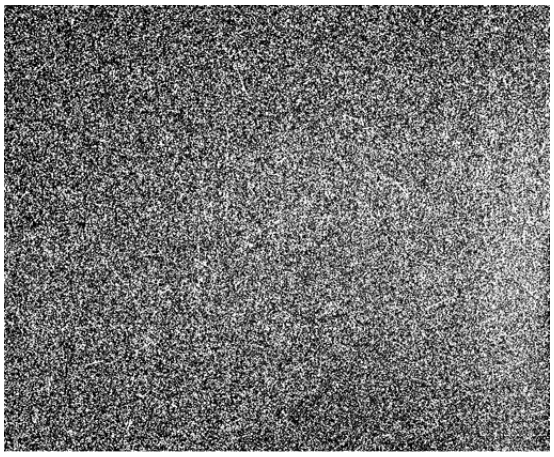

Figure 18. Binned 5x5 image of iaab18ynq. Glow extending from the right hand side indicates possible light leak.

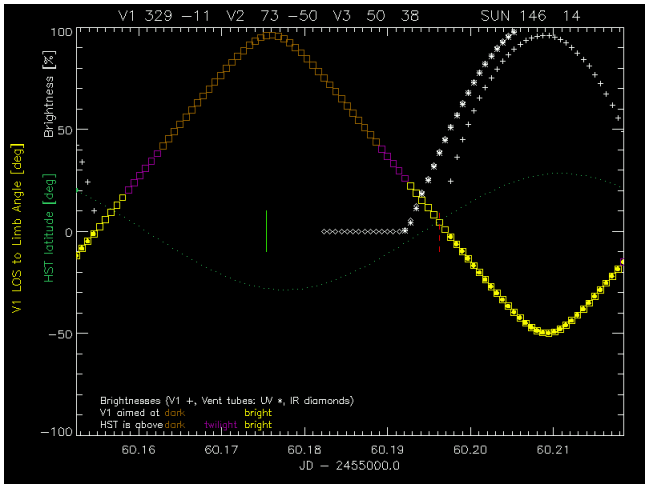

Figure 19. Plot showing HST's orientation with respect to Earth for image iaab18ynq.

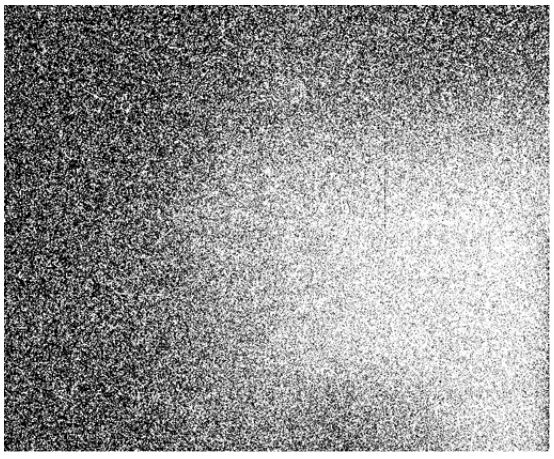

Figure 20. Binned 5x5 image of iaab19ynq. Faint glow extending from the right hand side indicating possible light leak.

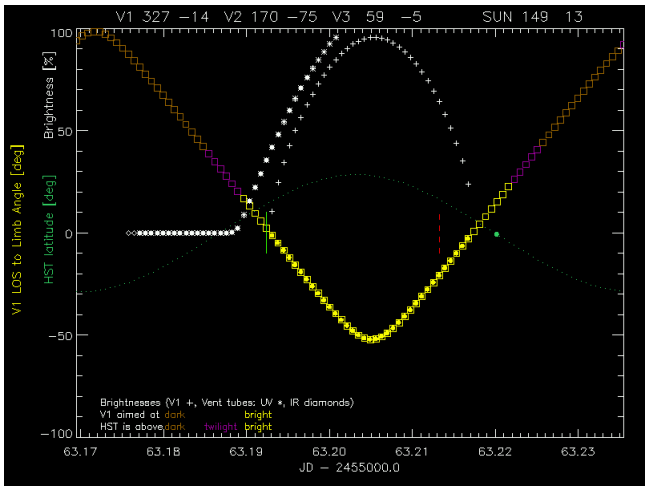

Figure 21. Plot showing HST's orientation with respect to Earth for image iaab19zwq.

Table 2. *List of images with elevated dark current: rootname, proposal id, date of observation, shutter blade, filter, the dark median (e-/pix/hr) for each chip, and a comment about HST pointed at bright Earth*

rootname	proposid	date-obs	shut	filter	median (e-/pix/hr) chip#1	median (e-/pix/hr) chip#2	comment
iaau02naq	11426	2009-06-26	A	F814W	4.62	4.65	7 min 2 sec in bright earth occultation
iaau32wtq	11426	2009-07-15	B	F814W	5.18	5.14	6 min and 7 sec in dark earth occultation
iaau52wxq	11426	2009-07-29	A	F814W	16.12	16.58	Entire exposure in bright earth occultation
iaab18ynq	11446	2009-08-16	B	F775W	4.64	4.98	Most of exposure in dark/bright earth occultation
iaab19zwq	11446	2009-08-19	A	F775W	14.49	14.77	Entire exposure in bright earth occultation

Hot Pixels

We chose a threshold for hot pixel cutoff of 20 e-/hr (0.0055 e-/s/pix = 6.6 DN/1800 sec), based on the tail of the dark histogram as well as a visual examination of the dark frames. Figure 23 shows a 200x200 pixel square where hot pixels above 20 e-/hr are identified with the red circles and green circles mark hot pixels above 60 e-/hr (20 DN in 1800 sec). We found that using a threshold of 60 e-/hr, the threshold chosen for ground data, was not sufficient to identify all hot pixels. Figure 22 shows a histogram from good (CR omitted) pixels for three images: the solid line represents a dark frame taken immediately after 1st anneal, the dashed line represents a dark frame taken 2 weeks after anneal, and the dotted line is about 4 weeks after anneal. A vertical line at 20 e-/hr is the hot pixel cutoff. At a threshold of 20 e-/hr, the rate for WFC3 hot pixels is 530 pix/day. Although the ACS dark current is also 5-10x higher than WFC3, at this limit, they find $\sim$430 new hot pix/day. For comparison, the threshold for hot pixel cutoff for ACS WFC is 144 e-/hr = 0.04e-/s = 96 DN/1800 sec.

In Figure 24 we plot the hot pixels as a fraction of the chip as a function of date for each dark measurement. The red dashed vertical line represent the anneals which occurred on June 23rd, July 20, and August 21. Note that prior to the first anneal the last darks were $\sim$10 days prior to the anneal due to the SIC&DH safing which occurred on June 15. The hot pixel removal from the anneal is $>70\%$ which is slightly less than the ACS hot pixel removal rate of $\sim82\%$ for WFC and $\sim86\%$ for HRC where "hot" pixels are classified as those with dark rate $>$0.08e-/pix/sec (see section 4.3.5 of ACS Instrument Handbook).

We report the number of hot pixels at various times after the anneal in Table 3. Table 4 shows the number of new hot pixels per day for various thresholds for the ACS WFC at -77 and -80C, the HRC at -81C, and WFC3. At ACS limit (144 e-/hr) the rate appears to decrease -6 pix/day and go up after an anneal. For reference, Table 5 provides a comparison of the different image characteristics for ACS and WFC3. Note that the hot pixel threshold used in this report was a preliminary value, chosen to flag both warm and hot pixels. A less stringent threshold will be used for future analysis for hot pixels, in order to better constrain the hot pixel tracking.

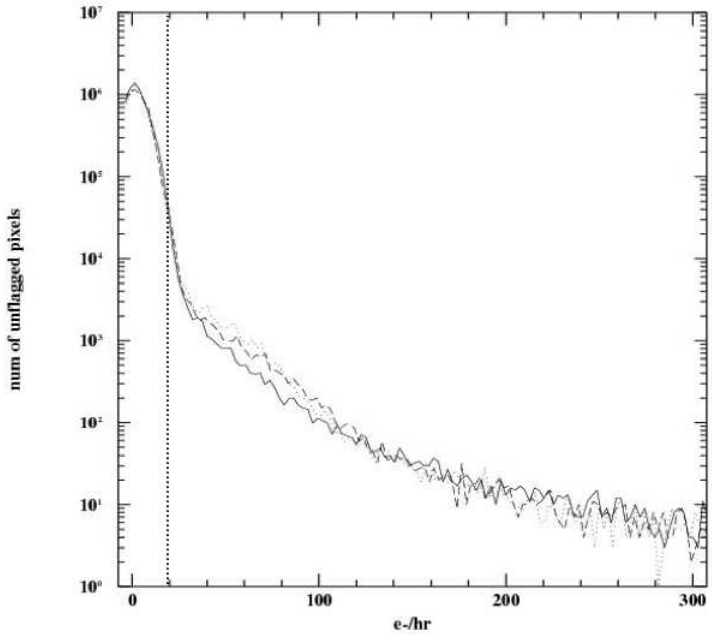

Figure 22. *Histogram from unflagged (CR-free) pixels for 3 images. The solid line immediately after 1st anneal, dashed line about 2 weeks after anneal, dotted line is about 4 weeks after anneal. The vertical line at 20 e-/hr is the hot pixel cutoff.*

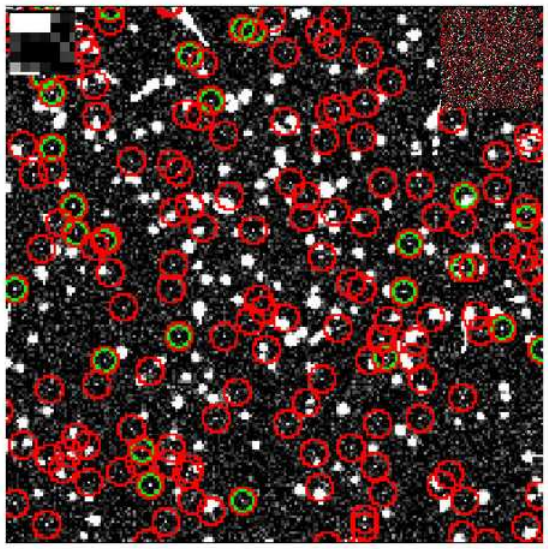

Figure 23. *Red circles mark hot pixels ID'd as above 20 e-/hr (6.6 DN in 1800 sec). Green circles mark hot pixels ID'd as above 60 e-/hr (20 DN in 1800 sec). Area shown is 200x200 pix square.*

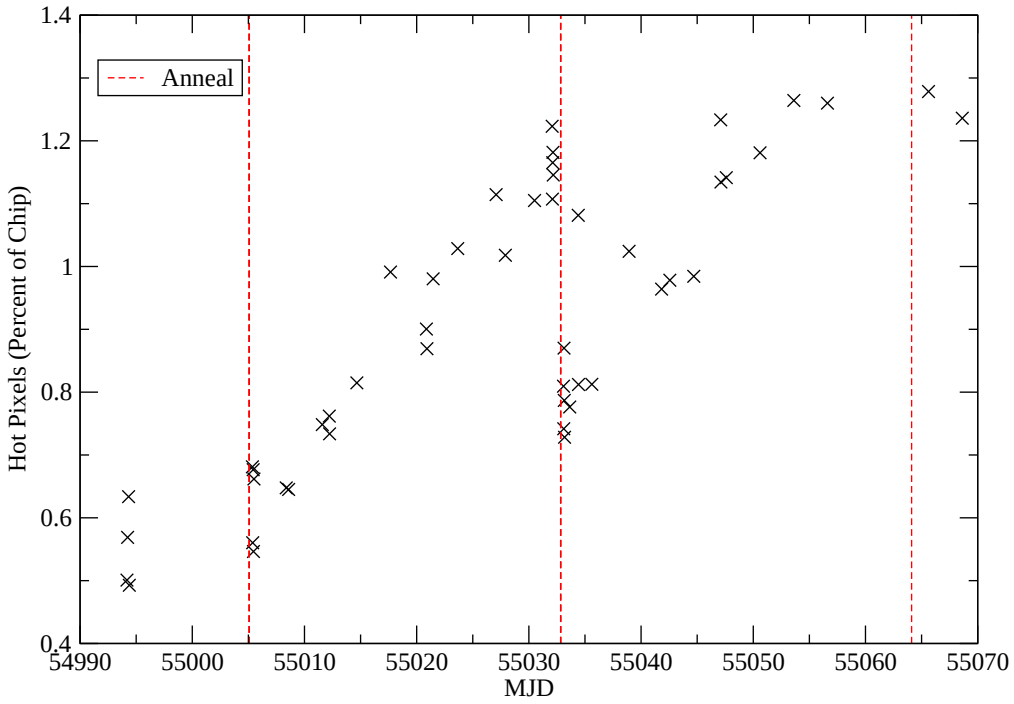

Figure 24. *Hot pixel growth between anneals. Anneals are represented by the vertical red dashed line where the first anneal occurred on June 23rd, the 2nd anneal on July 20, and the 3rd anneal on July 20. Hot pixel anneal rate is* $>70\%$.

Table 3. *Number of new hot pixels per day.*

Time Since Anneal	Number of hot pixels (pix/day)	Percent of chip
Immediately after anneal	54431	0.007%
14 days	67802	0.009%
28 days	68773	0.009%

On-orbit Superdark

On-orbit superdarks were created using SMOV data acquired between each anneal. Clean frames will be produced with *calwf3* and combined into superdarks as described

Table 4. *Number of new hot pixels per day for ACS and WFC3. Note that these numbers are for both chips.*

Thresh (e-/hr)	Thresh (e-/hr)	WFC (-77)	WFC (-80)	HRC (-81)	WFC3
20	0.0055	NA	NA	NA	1060
60	0.0167	NA	NA	NA	300
72	0.02	815 ± 56	NA	125 ± 12	NA
144	0.04	616 ± 22	427 ± 34	96 ± 2	-6
216	0.06	480 ± 13	292 ± 8	66 ± 1	
288	0.08	390 ± 9	188 ± 5	48 ± 1	
360	0.1	328 ± 8	143 ± 12	35 ± 1	
3600	1.00	16 ± 1	10 ± 1	1 ± 0.5	

Table 5. *Comparison of image formats of ACS and WFC3. The dark current for ACS WFC and HRC is the average value for WFC1 and WFC2 and the dark current for WFC3 is for both chips.*

Chip	Format	FOV	PIXSIZE	PIXSCALE	Dark Current (e-/pix/hr)	Readnoise (e-)
ACS-HRS	1024x1024	29"x26"	21 microns	$\sim$0.027"/pix	20.88	4.7
ACS-WFC	2x4096x2048	202"x202"	15 microns	$\sim$0.05"/pix	10.44	5.0
WFC3	2x4096x205	162"x162"	15 microns	$\sim$0.04"/pix	1.66	3.0

in WFC3 TIR 2008-01 (Martel et al.). Table 6 shows the statistics across the entire chip for the ground superdark using a 3 sigma clipping for two on-orbit superdarks. This tables includes the number of input frames, amplifiers, mean (e-/pix/hr) for both chips, standard deviation (DN) for both chips, and the number of hot pixels for both chips. On-orbit superdark d09062326 is a combination of 26 frames taken from June 23 - July 20 and d09072122 is a combination of 22 frames ranging from July 21 - August 19 2009. The ground superdark t3420177i_drk.fits, a combination of 4 x1000 sec exposures, has been reprocessed with the same *calwf3* version as the new on-orbit darks and the values reported are updated statistics from WFC3 ISR 2009-09 (Borders et al.). The dark current in the on-orbit superdark is $\sim$7x higher than the ground data. It should also be noted however, that the dark frames with elevated dark current were not removed from the creation of this superdark. Any superdark delivered to CDBS will exclude any dark frames with elevated dark current.

A greyscale image of the ground dark reference file (t3420177i_drk.fits), a full-frame four-amp image is shown in Figure 25. Figure 26 shows a greyscale image of the on-orbit stacked dark frame, a full-frame four-amp image of d09062326 and Figure 27 shows d09072122. The final dark reference file has overscans trimmed off, an exposure time of 1 sec, and is in units of e-/sec.

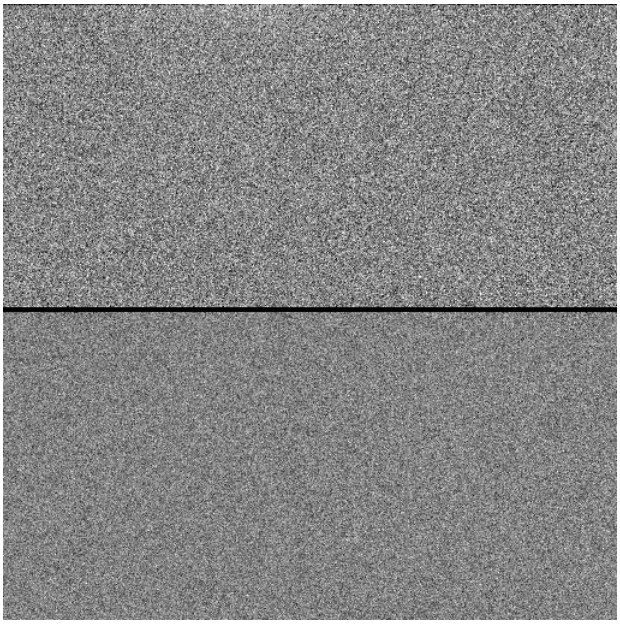

Figure 25. *Ground stacked dark file (4 x 1000 sec darks) t3420177i_drk.fits. Full frame two chip (A/B at top, C/D bottom).*

As can be seen in the on-orbit superdarks, there is a faint "glow" in the upper left corner of chip #1. This feature is not new and was observed in ground testing (see Fig. 2 of Martel 2008). This feature is also in the ground superdark but is not as visible with the grey scale stretch of the image in Figure 25.

Due to the extremely low dark current in the WFC3 detectors, initial plans for on-orbit superdarks delivered to CDBS are to set the normal pixels to zero, preventing the dark calibration from inserting extra noise into the science data. The warm and hot pixels will be retained in the dark reference file, allowing for *calwf3* DARKCORR step to calibrate these off-nominal pixels. On-orbit superdark reference files is to be installed and available via CDBS in January 2010.

Table 6. *On-orbit superdark statistics across the entire chip, using 3 sigma clipping.*

File	Number of Input Frames (Total Time)	Amplifiers	Mean (e-/pix/hr) (Chip #1, Chip #2)	Stddev (e-/pix/hr) (Chip #1, Chip #2)	Percent of Hot Pixels on Chip (Chip #1, Chip #2)
t3420177i_drk.fits	4 (1.11 hours)	ABCD	0.38, 0.31	5.55, 5.67	0.0009, 0.002
d09062326_drk.fits	26 (13 hours)	ABCD	2.02, 2.09	1.69, 1.66	0.08, 0.08
d09072122_drk.fits	22 (11 hours)	ABCD	2.26, 2.24	1.90, 1.87	0.11, 0.12

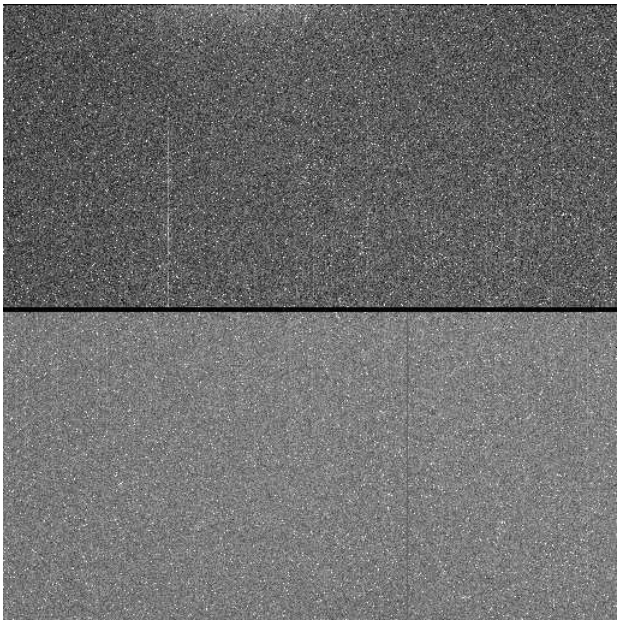

Figure 26. *On orbit stacked dark file (24 x 1800 sec darks) d09062326_drk. Full frame two chip (A/B at top, C/D bottom).*

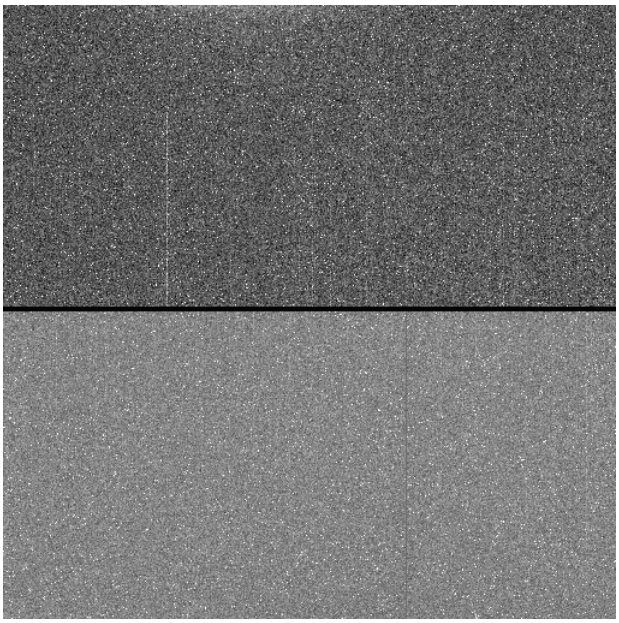

Figure 27. *On orbit stacked dark file (22 x 1800 sec darks) d09072122_drk . Full frame two chip (A/B at top, C/D bottom).*

Conclusions

Analysis of the UVIS dark frames for WFC3 in its on-orbit configuration shows the dark current to be 1.62 e-/pix/hr for chip#1 (amps A & B) and 1.70 e-/pix/hr for chip#2

(amps C & D). Approximately 5x higher than seen during ground tests but still much less than the CEI spec of 20 e-/pix/hr. In this report we investigate various checks and possible causes for the higher rate. The cause is not yet determined but a light leak around the shutter or radiation induced window glow are a leading candidate. In addition to the overall higher dark rate we found a number of extremely elevated darks. Our analysis shows that these highly elevated darks had both a red filter in place used for the preceding exposure as well as exposure to bright Earth. We determined the hot pixel cutoff to be 20 e-/hr based on the tail of histogram and measure a hot pixel rate of 530 pix/day. The annealing process fixes $>70\%$ of the hot pixels. For future analysis of hot pixels, a less stringent threshold will be used in order to better constrain hot pixel tracking.

Acknowledgements

Special thanks to R. Kimble, P.McCullough, J. MacKenty, L. Petro, T.Wheeler, and M. Wong and for their suggestions, comments, and discussions on the analysis of the darks.

References

Baggett, S., Borders, T., "WFC3 SMOV Proposal 11808: UVIS Bowtie Monitor."

Boffi, F.R., et al. 2007, "ACS Instrument Handbook", Version 8.0, (Baltimore: STScI).

Borders, T., Baggett, S., Martel, A.R., & Bushouse, H., 2009, WFC3 ISR 2009-09, "The WFC3/UVIS Reference Files: 3. Updated Biases and Darks."

Martel, A.R., Baggett, S., Bushouse, H., & Sabbi, E., 2008a, WFC3 TIR 2008-01, "The WFC3/UVIS Reference Files : 1. The Scripts," Available upon request.

Martel, A.R., Baggett, S., Bushouse, H., & Sabbi, E., 2009, WFC3 ISR 2008-42, "The WFC3/UVIS Reference Files : 2. Biases and Darks."

Martel, A.R., 2007, WFC3 ISR 2007-026, "WFC3 TV2 Testing: UVIS-2 Dark Frames and Rates."

Martel, A.R., 2008, WFC3 ISR 2008-022, "WFC3 TV3 Testing: UVIS-1' Dark Frames and Rates."

Aug 2009. Private communication with Tom Wheeler.

Appendix A.

Table 7. *List of observations: rootname, proposal id, date and time of observation, shutter blade, filter, and the dark median. All images are full-frame, four-amp readout 1800 sec dark frames.*

rootname	proposid	date-obs	time-obs	shut	filter	median (chip#1) e-/pix/hr	median (chip#2) e-/pix/hr
iaao01kaq	11419	2009-06-12	4:16:16	A	FQ889N	1.62	1.58
iaao02kgq	11419	2009-06-12	5:36:59	A	FQ889N	1.84	2.00
iaao03kqq	11419	2009-06-12	7:45:55	B	F475X	2.00	2.22
iaao04kwq	11419	2009-06-12	9:15:32	B	F475X	1.61	1.54
iaag03a6q	11431	2009-06-23	8:40:00	A	F475X	2.16	1.95
iaag03a9q	11431	2009-06-23	9:14:15	A	F475X	1.34	1.50
iaag03acq	11431	2009-06-23	10:17:34	A	F475X	1.69	2.06
iaag03afq	11431	2009-06-23	10:51:49	A	F475X	1.29	1.46
iaag03aiq	11431	2009-06-23	11:55:39	A	F475X	1.78	1.93
iaau02naq	11426	2009-06-26	8:30:22	A	F814W	4.62	4.65
iaau02ndq	11426	2009-06-26	9:02:30	A	F814W	1.63	1.49
iaab01o7q	11446	2009-06-26	14:08:27	B	F475X	1.48	1.35
iaab02b5q	11446	2009-06-29	14:08:26	B	F475X	1.78	1.75
iaau12gqq	11426	2009-06-30	5:04:56	A	F475X	1.41	1.63
iaau12gvq	11426	2009-06-30	5:37:04	A	F475X	1.70	1.41
iaab03s4q	11446	2009-07-02	16:03:44	A	F410M	1.65	1.77
iaab04oyq	11446	2009-07-05	16:03:33	B	F475X	1.44	2.11
iaau22ueq	11426	2009-07-08	20:46:20	B	F814W	1.78	1.51
iaau22upq	11426	2009-07-08	21:58:15	B	F814W	1.23	1.42
iaab05xdq	11446	2009-07-09	11:16:51	A	FQ619N	1.47	1.82
iaab06g6q	11446	2009-07-11	15:48:19	B	F475X	1.68	1.93
iaau32wrq	11426	2009-07-15	1:54:22	B	F814W	1.51	1.93
iaau32wtq	11426	2009-07-15	2:36:35	B	F814W	5.18	5.14
iaab07ajq	11446	2009-07-15	21:41:15	A	F606W	1.46	1.29
iaab08ofq	11446	2009-07-18	12:04:24	A	F438W	1.64	1.57
iaag04a2q	11431	2009-07-20	1:48:07	A	F475X	1.85	2.01
iaag04a7q	11431	2009-07-20	2:22:22	A	F475X	1.22	1.41
iaag04aiq	11431	2009-07-20	2:56:37	A	F475X	1.71	1.56
iaag04aoq	11431	2009-07-20	3:30:52	A	F475X	2.02	1.74

Table 8. *(Continued) List of observations: rootname, proposal id, date and time of observation, shutter blade, filter, and the dark median. All images are full-frame, four-amp readout 1800 sec dark frames.*

rootname	proposid	date-obs	time-obs	shut	filter	median (chip#1) e-/pix/hr	median (chip#2) e-/pix/hr
iaag04atq	11431	2009-07-20	4:05:07	A	F475X	1.73	1.60
iaag06dpq	11431	2009-07-21	1:59:59	B	F475X	1.77	1.61
iaag06dsq	11431	2009-07-21	2:34:14	B	F475X	1.11	1.10
iaag06dvq	11431	2009-07-21	3:08:29	B	F475X	2.08	2.30
iaag06e0q	11431	2009-07-21	3:42:44	B	F475X	1.18	1.52
iaag06e3q	11431	2009-07-21	4:16:59	B	F475X	1.67	1.17
iaab09ktq	11446	2009-07-21	15:20:05	B	F814W	1.18	1.66
iaau42naq	11426	2009-07-22	9:36:38	B	F475X	2.15	2.78
iaau42niq	11426	2009-07-22	10:08:46	B	F475X	1.60	1.62
iaab10cjq	11446	2009-07-23	14:41:16	A	F475X	1.63	1.27
iaab11amq	11446	2009-07-26	22:19:04	B	F475X	2.05	1.94
iaau52wvq	11426	2009-07-29	19:54:22	A	F814W	1.62	1.66
iaau52wxq	11426	2009-07-29	20:26:30	A	F814W	16.12	16.58
iaab12aoq	11446	2009-07-30	13:28:46	A	F275W	1.31	1.32
iaab13jkq	11446	2009-08-01	16:41:46	B	F625W	1.42	1.19
iaau62hlq	11426	2009-08-04	2:16:14	A	F475X	1.94	2.15
iaau62hnq	11426	2009-08-04	2:48:22	A	F475X	1.75	1.68
iaab14kvq	11446	2009-08-04	14:15:03	A	F336W	1.57	1.61
iaab15sdq	11446	2009-08-07	14:26:20	B	F775W	1.31	1.71
iaab16hcq	11446	2009-08-10	14:48:25	B	F475X	1.46	1.65
iaab17d2q	11446	2009-08-13	14:43:02	A	F775W	1.70	1.24
iaab18ynq	11446	2009-08-16	16:12:34	B	F775W	4.64	4.98
iaab19zwq	11446	2009-08-19	16:37:04	A	F775W	14.49	14.77
iaab20v6q	11446	2009-08-22	14:52:21	A	F218W	2.12	2.39
iaab21roq	11446	2009-08-25	15:03:37	A	F300X	1.79	2.06